Accepted Manuscript

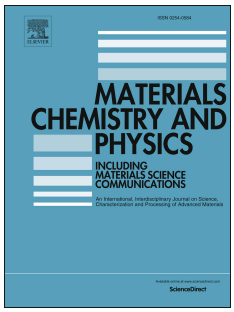

Synthesis and characterization of Al@MOF materials

Eirin Langseth, Ole Swang, Bjørnar Arstad, Anna Lind, Jasmina H. Cavka, Tomas Lunde Jensen, Tor Erik Kristensen, John Moxnes, Erik Unneberg, Richard H. Heyn

PII: S0254-0584(19)30014-8

DOI: https://doi.org/10.1016/j.matchemphys.2019.01.009

Reference: MAC 21279

To appear in: *Materials Chemistry and Physics*

Received Date: 12 June 2018

Revised Date: 25 October 2018

Accepted Date: 4 January 2019

Please cite this article as: E. Langseth, O. Swang, Bjø. Arstad, A. Lind, J.H. Cavka, T.L. Jensen, T.E. Kristensen, J. Moxnes, E. Unneberg, R.H. Heyn, Synthesis and characterization of Al@MOF materials, *Materials Chemistry and Physics* (2019), doi: https://doi.org/10.1016/j.matchemphys.2019.01.009.

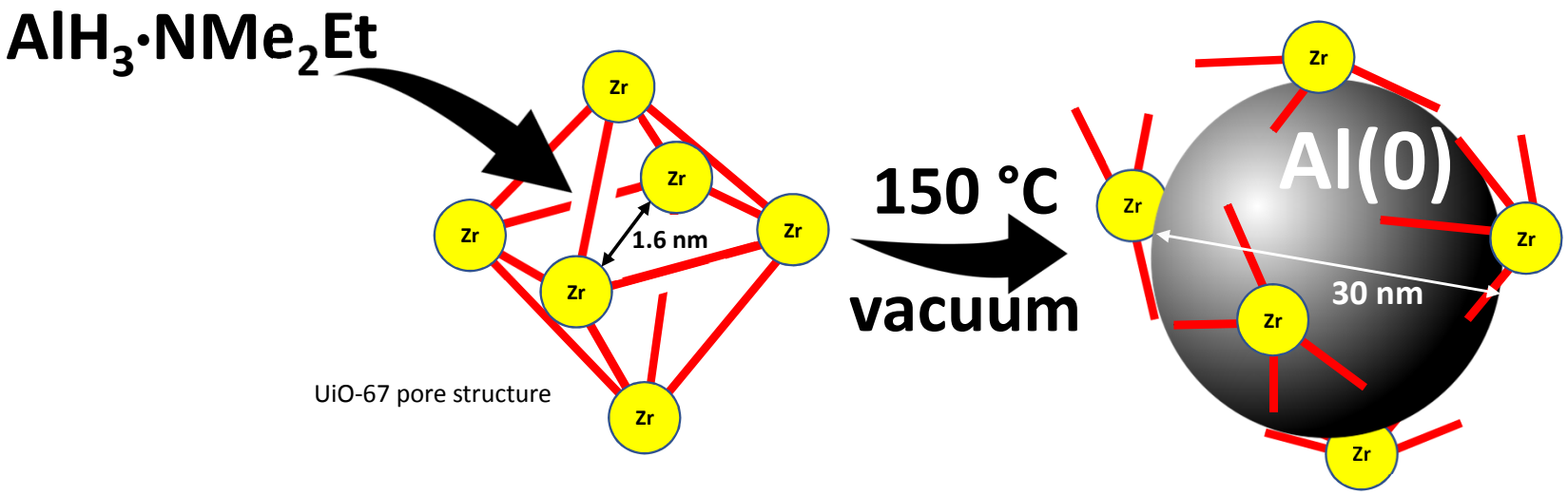
AlH3·NMe2Et
Zr
Zr
Zr
Zr
Zr
Zr
1.6 nm
UiO-67 pore structure
150 °C
vacuum
Zr
Zr
Zr
Zr
Zr
Al(0)
30 nm

Synthesis and Characterization of Al@MOF Materials

Eirin Langseth,[a,1] Ole Swang,[a,b] Bjørnar Arstad,[a] Anna Lind,[a] Jasmina H. Cavka,[a] Tomas Lunde Jensen,[c] Tor Erik Kristensen,[c] John Moxnes,[c] Erik Unneberg,[c] and Richard H. Heyn[a,*]

[a]SINTEF Industry, P. O. Box 124 Blindern, 0314 Oslo, Norway

[b]Department of Chemistry, University of Oslo, P. O. Box 1033 Blindern, 0315 Oslo, Norway

[c]Norwegian Defence Research Establishment, FFI, P. O. Box 25, 2027 Kjeller, Norway

[1]Current address: Jotun A/S, P. O. Box 2021, 3202 Sandefjord, Norway

Corresponding author: Richard H. Heyn, rhh@sintef.no

Abstract

The potential impregnation of Al(0) nanoparticles in the pores of three different metal-organic frameworks (MOFs), MIL-53-Al, HKUST-1, and UiO-67, was investigated through the suspension of the MOFs in AlH_3•NMe_2Et (**1**), followed by filtration, toluene wash, and heating to 150 °C under vacuum. Calculations based on the ratios of molecular and pore volumes provided idealized, benchmark impregnation capacities. Three successive impregnation cycles were performed to provide maximum incorporation of Al in the pores, and the materials were characterized after each impregnation cycle by ICP elemental analysis, BET surface area, and pore volume measurements. For MIL-53-Al, about half of the calculated amount of Al was incorporated into the MIL-53 pore structure, and PXRD data indicated a loss of crystallinity after the third incorporation cycle. Little Al incorporation was observed with HKUST-1, and the large decrease in surface area and pore volume, without significant change in the PXRD pattern, is attributed to pore blockage. Reaction of a large excess of **1** with UiO-67 was highly exothermic and evolved gas, likely from reaction with the μ_3-OH groups in the UiO-67 structure. The resulting material was amorphous apart from metallic Al(0) crystals approximately 30 nm in size and larger than the UiO-67 pores, as determined by PXRD and ^{27}Al MAS NMR spectroscopy. This material exhibited no apparent reaction with air or water and exposure to air gave little change in the ^{27}Al MAS NMR spectrum. The Al(0) crystals thus appear to be protected from oxidation, presumably by the remaining UiO-67 framework.

Keywords: MOF, aluminum, nanoparticle, impregnation

1. Introduction

Its large enthalpy of oxidation makes metallic aluminum a particularly useful component of energetic materials such as rocket propellents, explosives, and pyrotechnics. While lower ignition temperatures are observed with decreasing aluminum particle size, smaller particles also have a lower active metal content, as a greater fraction of the aluminum is present in the surface alumina layer with decreasing size [1]. Technology that provides easy Al(0) nanoparticle synthesis and that also protects the Al(0) against oxidation during formation of the final energetic material may potentially provide improved energetic materials. While several strategies for the passivation of Al nanoparticles toward oxidation have been investigated, including coatings made from other metals, carbon and various carboxylic acids [1], the use of porous materials as a passivation matrix towards oxidation has, to our knowledge, never been investigated.

Of the myriad porous materials that could be investigated, we chose metal-organic frameworks (MOFs). MOFs are a unique class of inorganic-organic hybrid materials built up from metal or metal oxide secondary building units (SBUs) and linked together by organic molecules (linkers) into a wide variety of porous structures. MOFs can therefore provide tunable and permanent porosities, with surface areas up to 5000 m^2/g, and research on the applications of these materials as absorbents, catalyst supports and sensors is evolving from academic curiosity to industrial implementation [2,3]. Additionally, the large, free and accessible cavities have led to research on composite MOF materials [4,5], whereby the introduction of metallic nanoparticles, carbon materials, organic polymers or even enzymes into the MOF pores provides improved, synergistic properties. The encapsulation or impregnation of various metallic and metal oxide nanoparticles is a particularly vibrant

research area for the development of improved catalysts, sensors, and separation materials [6,7].

While there are numerous reports on the encapsulation of transition metal or metal-oxide nanoparticles within MOFs, there are only two reports of aluminum-based nanoparticle-MOF composites, both on the use of the resulting composites for hydrogen storage. The impregnation of a solution of AlH_3•NMe_2Et (**1**) in toluene, followed by heating to 75 °C to dissociate the alane-amine adduct, gave a 1.4 % AlH_3 loading in the pores of a ZIF-8 structure and retention of crystallinity [8]. The reduction in surface area and pore volume compared to pristine ZIF-8 was from 1125 to 880 m^2/g and from 0.50 to 0.39 m^3/g, respectively. Similarly, tetrahydrofuran solutions of AlH_3 were used to impregnate the pores of MIL-101, and Al nanoparticles were generated in the pores via heating [9]. The maximum reduction of surface area and pore volume as compared to the starting MIL-101 was approximately 40 % with a loading of 1400 ppm Al. Particles of 2-5 nm diameter were observed with TEM for an Al loading of 925 ppm, although the oxidation state of the Al in the pores of the still crystalline material was not explicitly determined.

Atomic layer deposition chemistry of Al_2O_3 in MOFs has been studied with the Zr-based MOFs UiO-66-NH_2 [10] and NU-1000 [11,12,13]. For the former, exposure to alternating $AlMe_3$ and H_2O vapors led only to formation of an Al_2O_3 surface on the MOF. The lack of penetration into the pores was attributed to the similar dimensions of $AlMe_3$ and the UiO-66-NH_2 pore opening. For NU-1000, exposure of either $AlMe_3$ or $(AlMe_2O^iPr)_2$ vapor, followed by H_2O vapor, formed Al_2O_3 nanoclusters in the small (~0.8 nm) pores that are perpendicular to the large (3 nm diameter) pores in NU-1000 [14]. In both cases, diffuse reflectance infrared Fourier transform

(DRIFT) spectra and other experimental techniques showed that the Al precursors reacted with the bridging μ_3-OH hydroxyl and μ_3-O oxygen groups in the Zr_6 SBUs of the MOFs.

Our hypothesis was that MOFs would be suitable supports for the impregnation of Al(0) nanoparticles and that these Al@MOF composites would lead to improved energetic materials. Variations in the size and shape of the pores in different MOFs suggest related variations in the amount and form of the impregnated Al. This contribution describes our efforts to impregnate and characterize Al nanoparticles in three different MOFs.

2. Experimental

All syntheses were carried out under Ar in a dry box or with standard Schlenk techniques. AlH_3•NMe_2Et was purchased from SAFC Hitech and used as received. Toluene was either dried over Na and distilled or dried over molecular sieves. MIL-53-Al and HKUST-1 were purchased from Sigma-Aldrich. UiO-67 was prepared according to literature procedures, but at 90 °C rather than 120 °C [15]. All MOFs were activated at 150 °C under vacuum, overnight, prior to impregnation.

General synthetic procedure. The activated MOF was added to a Schlenk tube and **1** was added via syringe. The resulting suspension was stirred at room temperature for 16-19 h. The suspension was filtered on a filter frit to remove excess **1**, washed rapidly with toluene (ca 10 mL), and briefly dried under vacuum to provide a powder. The material was thereafter transferred to a new Schlenk tube and was heated to 150 °C under vacuum for at least 3 h. Details of the syntheses (amounts of reagents and products and observations) are provided in the Supplementary Material.

Simulated absorption capacities. Monte Carlo simulations of sorption capacities were carried out using the Sorption module of Accelrys Materials Studio version 6.1 [16]. The UFF forcefield

[17] was employed. After an equilibration run of 10^5 steps, production runs of 10^6 steps were performed. The molecular volume of **1** was computed according to Connolly [18], while the volume of an aluminum atom was calculated from the van der Waals radius (1.85 Å).

BET and pore volume measurements. Surface area and pore volume of all samples were measured by N_2 adsorption at 77 K using the manometric unit Belsorp-mini. The samples were pretreated directly in the apparatus under vacuum at 100 °C for 2 h. Fresh samples were activated in an external apparatus at 150 °C under vacuum overnight prior to the measurements. The Brunauer-Emmett-Teller (BET) formula was used for determination of surface area and Barrett-Joyner-Halenda (BJH) formula for pore volume analysis.

Elemental analysis. Elemental analyses were carried out on a Thermo X-series II ICP-MS (inductively coupled plasma mass spectrometer). Prior to analysis, 0.01 g of each sample was digested in 3 mL nitric acid (ultrapure 67-70 %) and 6 mL hydrochloric acid (suprapure 30 %) in a Teflon® tube, followed by pressurization in a microwave oven (UlltraWAVE, Milestone). The samples were heated to 260 °C for 10 min and then cooled. The metals were quantified according to a standard curve (four points). Certified reference materials from Environmental Canada (TM-23.4, Bigmoose-02, TMDA-61.2 and Battle-2) were analyzed to obtain good accuracy. An internal standard was injected together with the samples to ensure high analytical precision.

NMR spectroscopy. Two experiments with **Al@UiO-67-1A** were performed, one on a sample prepared under inert atmosphere, and the second on a sample prepared in air. The ^{27}Al MAS NMR experiments were carried out at room temperature at a magnetic field of 11.7 T (^{27}Al resonance frequency of 130.31 MHz) using a 4 mm double resonance probe head. The MAS rate was 12 kHz. The spectra were generated from 12000 single pulse transients for the inert sample and 3000 single pulse transients for the air sample.

Powder X-ray diffraction (PXRD) measurements. PXRD data were collected on a PANalytical Empyrean diffractometer equipped with a PIXcel3D solid state detector. The measurements were carried out in reflection geometry using CuK_α radiation (λ = 1.541874 Å) and a step size of 0.013 degrees. The PXRD patterns were recorded over a 2θ range of 5-100° with a scan speed of 0.05 °/s. Samples for PXRD analysis were prepared in air. The PXRD of MIL-53-Al was simulated from the single crystal structure of MIL-53-Al-*ht* phase [19] using the freeware version of Mercury 3.9 from the Cambridge Crystallography Data Centre https://www.ccdc.cam.ac.uk/. The Al crystal size was estimated by the line profile analysis (LPA) in the PANalytical HighscorePlus software. Reference XRD data provided in the Supplementary Material (Tables S1-S4) are obtained from the Crystallography Open Database (COD) http://www.crystallography.net/cod/.

3. Results and Discussion

Three different MOFs were chosen for the impregnation studies: MIL-53-Al, HKUST-1, and UiO-67. These were chosen on the basis of their pore structure and the calculated amount of Al that could be impregnated (*vide infra*). MIL-53-Al, $[Al(OH)(O_2C\text{-}C_6H_4\text{-}CO_2)]_n$, consists of $AlO_4(OH)_2$ octahedra interconnected by 1,4-benzenedicarboxylate groups, that create one-dimensional (1D) channels of 0.85 x 0.85 nm^2 upon evacuation of guest molecules. It has a breathing type structure; the pores can decrease or increase in size depending on the guest molecules present [19]. HKUST-1, also known as CuBTC, has Cu_2-clusters η^1,η^1-bonded to four carboxylate groups, each from a benzene-tricarboxylic acid (BTC; trimesic acid) linker, in a paddlewheel geometry. The BTC linkers create a three-dimensional (3D) cubic network with distances of 1.1 and 1.6 nm between the Cu_2-clusters [20,21]. UiO-67 is formed by $Zr_6(OH)_4O_4$ clusters linked by biphenyl-4,4'-dicarboxylate units. This construction provides a 3D cubic

network with 1.2 and 1.6 nm diameter pores [15]. The surface areas and pore volumes of the different MOFs after activation are given in Table 1.

A solution impregnation method [5] was used for the material syntheses. **1** was chosen as the precursor, since this substrate can be easily reduced to Al(0) by simple heating to at least 100 °C at low pressure ($2.4 \cdot 10^{-4}$ Torr) [22]. Also, since **1** is a liquid, it was used without additional solvents, in contrast to the previous studies on the impregnation of alane into MOFs, which utilized toluene and THF solutions of **1** and AlH_3, respectively [8,9]. The general procedure involved immersion of the MOF material in an excess of **1** with stirring, isolation of the new material by filtration, a quick, yet thorough wash with toluene, and finally removal of residual toluene under vacuum. Both the washing and the drying steps were performed quickly to minimize the removal of any **1** from the pores of the MOF. Reduction of **1** to Al(0) was performed by simply heating the isolated material to 150 °C under vacuum for 3 h.

3.1 Modelling of the maximum Al incorporation

Prior to any material synthesis, the maximum impregnation of Al in each MOF was determined computationally to provide a benchmark for the synthetic experiments. First, the absorption capacity of **1** in each MOF was computed by both Monte Carlo (MC) simulations and molecular and pore volume calculations, under the assumption that **1** remained an intact adduct within the MOF pores during absorption. The volume approach involved the calculation of the pore volume of the MOF and the molecular volume of **1**, and the loading was calculated simply as the ratio of volumes. A comparison of these two methods for the absorption of **1** into each of the three MOFs is given in Table 2. The two methods give very similar results, with the discrepancies within the same order of magnitude that could be expected from the approximations in the calculations (perfect crystals without external surfaces and an empirical

forcefield). Particularly, the MOF with the largest pore volume, UiO-67, gave essentially identical results. Hence, the volume ratio approach was used to estimate the adsorption capacities for subsequent impregnations.

Since **1** is larger than an Al atom, it was reasoned that multiple impregnation cycles, *i.e*. absorption of **1** and reduction to Al(0), would permit greater amounts of Al within the pores. Assuming total reduction of **1** to Al(0), the amount of **1** that could be incorporated into the remaining volume (pore volume – volume of the previously impregnated Al(0)) in subsequent impregnation cycles was calculated. For these calculations, the atomic volume of Al(0) was used. Thus, the amount of Al(0) present in the pores of the MOFs after each of three successive impregnation cycles was calculated. The results of these idealized impregnation cycles are given in Table 3 in terms of the number of Al atoms that can be incorporated into each MOF unit cell, and the number of Al atoms per SBU metal atom in each MOF unit cell. After the third impregnation cycle, MIL-53-Al and HKUST-1 have a modelled impregnation capacity of one Al(0) atom per metal atom in the MOF SBU, while UiO-67 has room for at least four Al(0) atoms for each Zr atom in the $Zr_6(OH)_4O_4$ SBU cluster.

3.2 Impregnation in MIL-53-Al

The results of the ICP elemental analyses and BET and pore volume measurements of the materials after each of three successive impregnation cycles in MIL-53-Al are shown in Table 4. Since both the metal in the MOF SBU and the impregnated metal are Al, the change in the wt % Al in the ICP data, as compared to unimpregnated MIL-53-Al, is attributed to the impregnated Al. Impregnation of **1** into MIL-53-Al and subsequent reduction gave a distinctly darker material than the starting MIL-53-Al. None of the **Al@MIL-53** materials exhibited reactivity with air or water.

The amount of Al incorporated into MIL-53-Al after three impregnation cycles is about half that of the calculated value. No further incorporation of Al was observed in the final impregnation cycle, and the changes in the surface area and pore volume between cycles are irregular. A plausible explanation relates to the breathing motif exhibited by MIL-53-Al. Activation of MIL-53-Al removes all guest molecules and forms the large pore version of the material, MIL-53-Al-*ht* [19]. Reintroduction of guest molecules generates dipole moment interactions between the host framework and these molecules, resulting in a narrowing of the pores and subsequent reduction of the available pore volume. This effect has been observed for H_2O, CO_2, and synthesis solvent molecules [23], and it can be imparted to the **Al@MIL-53** materials by the position, size, and chemical nature of the impregnated Al and any residual NMe_2Et, for example coordinated to open sites at the lattice Al atoms. The PXRD of **Al@MIL-53-3** (Figure 1) shows diffraction peaks consistent with the original structure, although these are significantly broader, and the diffractogram contains additional peaks and amorphous features. An explanation for these observations is the reaction of **1** with the Al-OH-Al moieties closest to the pore openings, leading to decomposition and pore blockage, thus inhibiting impregnation further within the 1D pores.

3.3 Impregnation in HKUST-1

The ICP analyses, BET results and pore volume measurements of the materials from three successive impregnations in HKUST-1 are shown in Table 5. As with MIL-53, addition of **1** to HKUST-1 gave materials with a darker color. The dark blue color of impregnated HKUST-1 was maintained as long as the materials were kept under inert conditions. Exposure to air or water did not yield any apparent reaction, although the materials returned to a blue-turquoise color similar to unactivated HKUST-1. The lightening in color has been attributed to the coordination of Lewis bases at the Cu centers of the framework [20].

The data for the material from the first impregnation cycle, **Al@HKUST-1**, suggest successful incorporation of Al into the HKUST-1 pores, although the amount of Al impregnated is less than half the maximum calculated value. However, the second impregnation gave a significant reduction in the surface area and pore volume of the material without any concomitant increase in the amount of Al. Likewise, the third impregnation provided a similar, small increase in the amount of Al and resulted in a nearly non-porous material. In contrast to MIL-53-Al and its Al-OH-Al groups, HKUST-1 does not contain any Brønsted acid sites for reaction with AlH_3 and only the weakly Lewis basic carboxylate O atoms for coordination to Al. The PXRD pattern of **Al@HKUST-3** (Figure 2), after the final impregnation of Al, shows that the crystallinity of the host MOF was essentially retained, although the diffraction peaks and background are broadened. A plausible explanation for the large decrease in surface area and pore volume, and a slightly more amorphous structure, without a large amount of impregnated Al is the deposition of Al or Al_2O_3 primarily around the pore openings of HKUST-1, which would prevent impregnation while disrupting only the long-range crystalline order.

3.4 Impregnation in UiO-67

The addition of **1** to activated UiO-67 resulted in an immediate exothermic reaction characterized by liquid evaporation (presumably NMe_2Et) and gas evolution. Addition of 90 equiv **1** to UiO-67 (as determined by the number of $[Zr_6O_4(OH)_4(O_2C\text{-}C_6H_4\text{-}C_6H_4\text{-}CO_2)_6]$ formula units) resulted in the complete absorption of all **1** and gave a material **Al@UiO-67-1** with only 1 % of the original UiO-67 surface area and an 87 % reduction in pore volume. The ICP elemental analysis reveals incorporation of 17 Al atoms per Zr atom (Table 6), four times greater than that predicted from the modelling. A second impregnation with approximately 80 equiv **1** provided the material **Al@UiO-67-2** in a less intense exothermic reaction and with much smaller changes in the material characteristics. The relative lack of remaining surface

area and pore volume discouraged a third impregnation cycle. The immediate and observable reactivity between **1** and UiO-67 is attributed to the reaction of AlH_3 with the acidic μ_3-OH groups, and perhaps other oxygen functionalities, present in the $Zr_6O_4(OH)_4(CO_2)_6$ SBUs of UiO-67, as has been shown by the discrete deposition of $AlMe_3$, $InMe_3$, and $ZnEt_2$ at these sites in NU-1000 [12,13,14]. In contrast to the other reagents, the reaction with $AlMe_3$ did not show self-limiting behavior, and prolonged exposure of $AlMe_3$ to NU-1000 showed a significant loss of crystallinity [12].

Since all of **1** was absorbed in the synthesis of **Al@UiO-67-1**, the first impregnation cycle was repeated. The addition of a very large excess of **1** to UiO-67 (> 700 equiv **1** per UiO-67 formula unit) resulted again in an exothermic reaction. On the basis of the ICP elemental analysis, the resulting material **Al@UiO-67-1A** contained 44 Al atoms per Zr atom, over ten times that predicted by modelling, which is equivalent to 264 Al atoms per UiO-67 formula unit and over 1000 Al atoms per UiO-67 unit cell. Correspondingly, the surface area and pore volume of **Al@UiO-67-1A** were reduced by more than 99 % and 94 %, respectively, compared to those of UiO-67. The large degree of impregnation can be explained by a breakdown of the UiO-67 pore structure, which would allow [24] a more extensive impregnation of **1** into UiO-67 than that predicted from calculations. Indeed, the PXRD pattern (Figure 3) shows that the regular, crystalline structure of UiO-67 had been destroyed, as evidenced by the broad, amorphous peaks for the MOF at $2\theta < 30°$. The pattern, however, provides distinct evidence for the presence of metallic Al(0) crystals approximately 30 nm in size, significantly larger than the 1.6 nm pores within UiO-67. The presence of Al(0) was further confirmed by the ^{27}Al MAS NMR spectrum (Figure 4), that shows an intense, characteristic signal at 1640 ppm [25]. The spectrum also contains a set of weak signals at approximately 7, 43 and 61 ppm, integrating to a total of about 1 % that of the Al(0) signal. These ppm values are very close to those observed

for AlO_4, AlO_5 and AlO_6 units in Al-NU-1000 (4.5, 35 and 68 ppm, respectively) [11]. The NMR data therefore strongly suggest that the impregnation chemistry has provided Al(0) crystals in close contact with the Zr_xO_y clusters from UiO-67, and not an Al crystal with a protective Al_2O_3 layer. Specifically, the Al(III)/Al(0) molar ratio of a 30 nm Al(0) nanoparticle coated with a 2.5 nm thick Al_2O_3 layer is calculated to be 0.4 (see Supplementary Material), a value that is inconsistent with the observed NMR data, even taking the inherent errors in integrating quadrupolar NMR signals into account. A thermal gravimetric analysis (TGA) of **Al@UiO-67-1A** under air (Supplementary Material) showed a weight increase starting near the melting point of Al (660 °C), consistent with the formation of Al_2O_3. Despite the destruction of the UiO-67 framework, the observations and data indicate that the remaining UiO-67 framework protects the Al(0) crystals from spontaneous oxidation upon exposure to air. **Al@UiO-67-1A** did not exhibit any apparent reactivity with air or water. The PXRD sample was prepared in air, without any observation of Al_2O_3 in the pattern. Finally, a ^{27}Al MAS NMR spectrum (see Supplementary Material) was recorded on a sample that was prepared and measured in air, and the intensity of the AlO_x signals were only 3-4 % larger than the corresponding signals in the original spectrum. While the AlO_x signals are slightly more intense, they are still much weaker than those expected for an Al_2O_3 layer around an Al(0) crystal.

4. Conclusions

A simple solution absorption and reduction method has been investigated for the impregnation of metallic Al(0) nanoparticles in the pores of three different MOFs, MIL-53-Al, HKUST-1 and UiO-67. Calculations of molecular and pore volumes provided benchmarks for the maximum incorporation of the Al(0) nanoparticles into the pristine MOF networks. The impregnation chemistry was more complex. The data collected after the third impregnation cycle in MIL-53-Al gave evidence of Al incorporation together with a loss of crystallinity. This

likely resulted from the blockage of the outer fraction of the 1D MIL-53-Al pores from reaction of **1** with the MOF's Al-OH-Al groups. The results of the attempted impregnation in HKUST-1 suggest the formation of materials with pores blocked by Al(0) or Al_2O_3; little Al was incorporated, the surface area and pore volume were significantly reduced, yet the HKUST-1 crystallinity was in general maintained. The exact chemical nature of the small amounts of Al impregnated in these MOFs was not investigated. For UiO-67, the reaction with **1** was immediate and exothermic, from reaction with the acidic μ_3-OH groups in the Zr_6 nodes of UiO-67. While the reaction led to the breakdown of the UiO-67 structure and loss of MOF crystallinity, the ^{27}Al MAS NMR and PXRD data confirm the formation of Al(0) crystals approximately 30 nm in size, much larger than the pore diameters available in UiO-67. The **Al@UiO-67-1A** material, however, was resistant to reaction with air or water, suggesting that the residual UiO-67 network protects the Al(0) crystals against further oxidation. The nature of this passivation phenomenon, greater control and understanding of the impregnation chemistry and the potential of these materials to enhance the performance of energetic materials may be subjects for further investigations.

5. Supplementary Material

Experimental details of the material syntheses and the TGA studies, calculations of the Al(III)/Al(0) molar ratio for Al(0) nanoparticles with an Al_2O_3 layer, TGA of UiO-67 under N_2 and **Al@UiO-67-1A** under air, ^{27}Al MAS NMR spectrum of **Al@UiO-67-1A** prepared and measured in air, absorption-desorption isotherms for all precursor and synthesized materials, and reference X-ray diffraction data for MIL-53-Al, HKUST-1, UiO-67, and aluminum.

6. Acknowledgements

We would like to thank Aud I. Spjelkavik (SINTEF) for her help with the absorption-desorption isotherms, Aud M. Bouzga (SINTEF) for her help with the NMR analyses, and Ida Vaa Johnson (FFI) for her help with the ICP analyses.

This research did not receive any specific grant from funding agencies in the public, commercial or not-for-profit sectors.

Declarations of interest: None.

7. References

[1] D. Sundaram, V. Yang, R. A. Yetter, Progr. Energy Combust. Sci. 61 (2017) 293-365.

[2] B. Li, H.-M. Wen, Y. Cui, W. Zhou, G. Qian, B. Chen, Adv. Mater. 28 (2016) 8819-8860.

[3] P. Silva, S. M. F. Vilela, J. P. C. Tome, F. A. Almeida Paz, Chem. Soc. Rev. 44 (2015) 6774-6803.

[4] S. Li, F. Hou, Nanoscale 7 (2015) 7482-7501.

[5] Q.-L. Zhu, Q. Xu, Chem. Soc. Rev. 43 (2014) 5468-5512.

[6] Q.-L. Zhu, Q. Xu, Chem 1 (2016) 220-245.

[7] P. Falcaro, R. Ricco, A. Yazdi, I. Imaz, S. Furukawa, D. Maspoch, R. Ameloot, J. D. Evans, C. J. Doonan, Coord. Chem. Rev. 307 (2016) 237-254.

[8] E. M. Banach, H. A. Stil, H. Geerlings, J. Mater. Chem. 22 (2012) 324-327.

[9] P. K. Prabhakaran, L. Catoire, J. Deschamps, Microporous Mesoporous Mater. 243 (2017) 214-220.

[10] P. C. Lemaire, D. T. Lee, J. Zhao, G. N. Parsons, ACS Appl. Mater. Interfaces 9 (2017) 22042-22054.

[11] M. Rimoldi, V. Bernales, J. Borycz, A. Vjunov, L. C. Gallington, A. E. Platero-Prats, I. S. Kim, J. L. Fulton, A. B. F. Martinson, J. A. Lercher, K. W. Chapman, C. J. Cramer, L. Gagliardi, J. T. Hupp, O. K. Farha, Chem. Mater. 29 (2017) 1058-1068.

[12] I. S. Kim, J. Borycz, A. E. Platero-Prats, S. Tussupbayev, T. C. Wang, O. K. Farha, J. T. Hupp, L. Gagliardi, K. W. Chapman, C. J. Cramer, A. B. F. Martinson, Chem. Mater. 27 (2015) 4772-4778.

[13] J. E. Mondloch, W. Bury, D. Fairen-Jimenez, S. Kwon, E. J. DeMarco, M. H. Weston, A. A. Sarjeant, S. T. Nguyen, P. C. Stain, R. Q. Snurr, O. K. Farha, J. T. Hupp, J. Am. Chem. Soc. 135 (2013) 10294-10297.

[14] L. C. Gallington, I. S. Kim, W.-G. Liu, A. A. Yakovenko, A. E. Platero-Prats, Z. Li, T. C. Wang, J. T. Hupp, O. K. Farha, D. G. Truhlar, A. B. F. Martinson, K. W. Chapman, J. Am. Chem. Soc. 138 (2016) 13513-13516.

[15] J. H. Cavka, S. Jakobsen, U. Olsbye, N. Guillou, C. Lamberti, S. Bordiga, K. P. Lillerud, K. P. J. Am. Chem. Soc. 130 (2008) 13850-13851.

[16] Materials Studio 6.1, Accelrys Software, Inc., 2012. R. L. C. Akkermans, N. A. Spenley, S. H. Robertson, Mol. Simul. 39 (2013) 1153-1164.

[17] A. K. Rappé, C. J. Casewit, K. S. Colwell, W. A. Goddard III, W. M. Skiff, J. Am. Chem. Soc. 114 (1992) 10024-10035.

[18] M. L. Connolly, J. Appl. Crystallogr. 16 (1983) 548-558.

[19] T. Loiseau, C. Serre, C. Huguenard, G. Fink, F. Taulelle, M. Henry, T. Bataille, G. Férey, Chem. Eur. J. 10 (2004) 1373-1382.

[20] K. Schlichte, T. Kratzke, S. Kaskel, Microporous Mesoporous Mater. 73 (2004) 81-88.

[21] S. S. Y. Chui, S. M. F. Lo, J. P. H. Charmant, A. G. Opren, I. D. Williams, Science 283 (1999) 1148-1150.

[22] M. G. Simmonds, I. Taupin, W. L. Gladfelter, Chem. Mater. 6 (1994) 935-942.

[23] M. Alhamami, H. Doan, C.-H. Cheng, Materials 7 (2014) 3198-3250.

[24] R. J. Marshall, R. S. Forgan, R. S. Eur. J. Inorg. Chem. (2016) 4310-4331.

[25] I. Nuta, E. Veron, G. Matzen, C. Bessada, Inorg. Chem. 50 (2011) 3304-3312.

Tables

Table 1. Measured surface areas, pore volumes, and thermal stabilities of the MOFs.

MOF	Surface area (BET, m^2/g)	Pore volume (cm^3/g)	Thermal stability (°C)
MIL-53-Al	1090	1.25	500[a]
KHUST-1	1706	0.75	260[b]
UiO-67	2187	1.33	450[c]

[a] Ref [19]. [b] Ref [20]. [c] Ref [15].

Table 2. Calculated absorption capacity of **1** in each MOF.

MOF	**SBU Metal atoms/unit cell**	**Molecules of 1/unit cell**	**1/SBU Metal atom**
MIL-53-Al	32		
MC simulation[a]		24	0.70
Volume ratios[b]		15	0.47
HKUST-1	48		
MC simulation		28	0.50
Volume ratios		20	0.42
UiO-67	24		
MC simulation		44	1.8
Volume ratios		44	1.8

[a] Monte Carlo simulations. [b] Calculated from ratios of the volumes of **1** and MOF pores.

Table 3. Calculated impregnation capacity of Al(0) in each MOF after each of three successive absorption and reduction steps cycles, via the volume ratio method.

	MIL-53-Al		**HKUST-1**		**UiO-67**	
Capacity	**Al/unit cell**	**Al/M[a]**	**Al/unit cell**	**Al/M[a]**	**Al/unit cell**	**Al/M[a]**
Cycle 1	15	0.47	20	0.42	44	1.8
Cycle 2	12	0.37	16	0.33	34	1.4
Sum of cycles 1 - 2	27	0.84	36	0.75	78	3.2
Cycle 3	10	0.31	13	0.27	27	1.1
Sum of cycles 1 - 3	37	1.16	49	1.02	105	4.3

[a] The ratio of Al(0) atoms to the number of SBU metal atoms (M) in each unit cell of the MOF.

Table 4. Analytical data for MIL-53-Al and the three Al@MIL-53 materials.

Material	ICP[a]		BET	Pore volume	Reduction in pore
	Al (wt %)	Al/M molar ratio	(m^2/g)	(cm^3/g)	volume (%)
MIL-53-Al	12	-	1102	1.25	-
Al@MIL-53-1	15	0.25	413	0.78	38
Al@MIL-53-2	18	0.50	374	0.77	38
Al@MIL-53-3	18	0.50	305	0.86	31

[a] The errors in the ICP data are estimated to be between 5-10 %.

Table 5. Analytical data for HKUST-1 and the three Al@HKUST-1 materials.

Material	ICP[a]			BET	Pore volume	Reduction in
	Al (wt %)	Cu (wt %)	Al/Cu[b]	(m^2/g)	(cm^3/g)	pore volume (%)
HKUST-1	-	28	-	1706	0.75	-
Al@HKUST-1	1.9	24	0.19	1389	0.59	21
Al@HKUST-2	2.6	24	0.25	197	0.10	87
Al@HKUST-3	3.1	23	0.30	50	0.04	95

[a] The errors in the ICP data are estimated to be between 5-10 %. [b] Molar ratio.

Table 6. Analytical data for UiO-67 and the three Al@UiO-67 materials.

Material	ICP[a]			BET	Pore volume	Reduction in
	Al (wt %)	Zr (wt %)	Al /Zr[b]	(m^2/g)	(cm^3/g)	pore volume (%)
UiO-67	-	23	-	2187	1.33	-
Al@UiO-67-1	42	8.2	17	21	0.17	87
Al@UiO-67-2	46	7.2	22	14	0.11	92
Al@UiO-67-1A	62	4.7	44	7	0.08	94

[a] The errors in the ICP data are estimated to be between 5-10 %. [b] Molar ratio.

Figure captions

Fig. 1 PXRD of MIL-53-Al and **Al@MIL-53-3**. The peaks marked with the red dots have been correlated with specific crystal planes, see Table S1 in the Supplementary Material.

Fig. 2 PXRD of HKUST-1 and **Al@HKUST-3**. The peaks marked with the red dots have been correlated with specific crystal planes, see Table S2 in the Supplementary Material.

Fig. 3 PXRD patterns of **Al@UiO-67-1A**, metallic Al and activated UiO-67. The peaks marked with the red dots have been correlated with specific crystal planes, see Table S3 in the Supplementary Material. The peaks marked with the green dots have been correlated with specific crystal planes, see Table S4 in the Supplementary Material.

Fig. 4 ^{27}Al MAS NMR spectrum of **Al@UiO-67-1A** under inert conditions

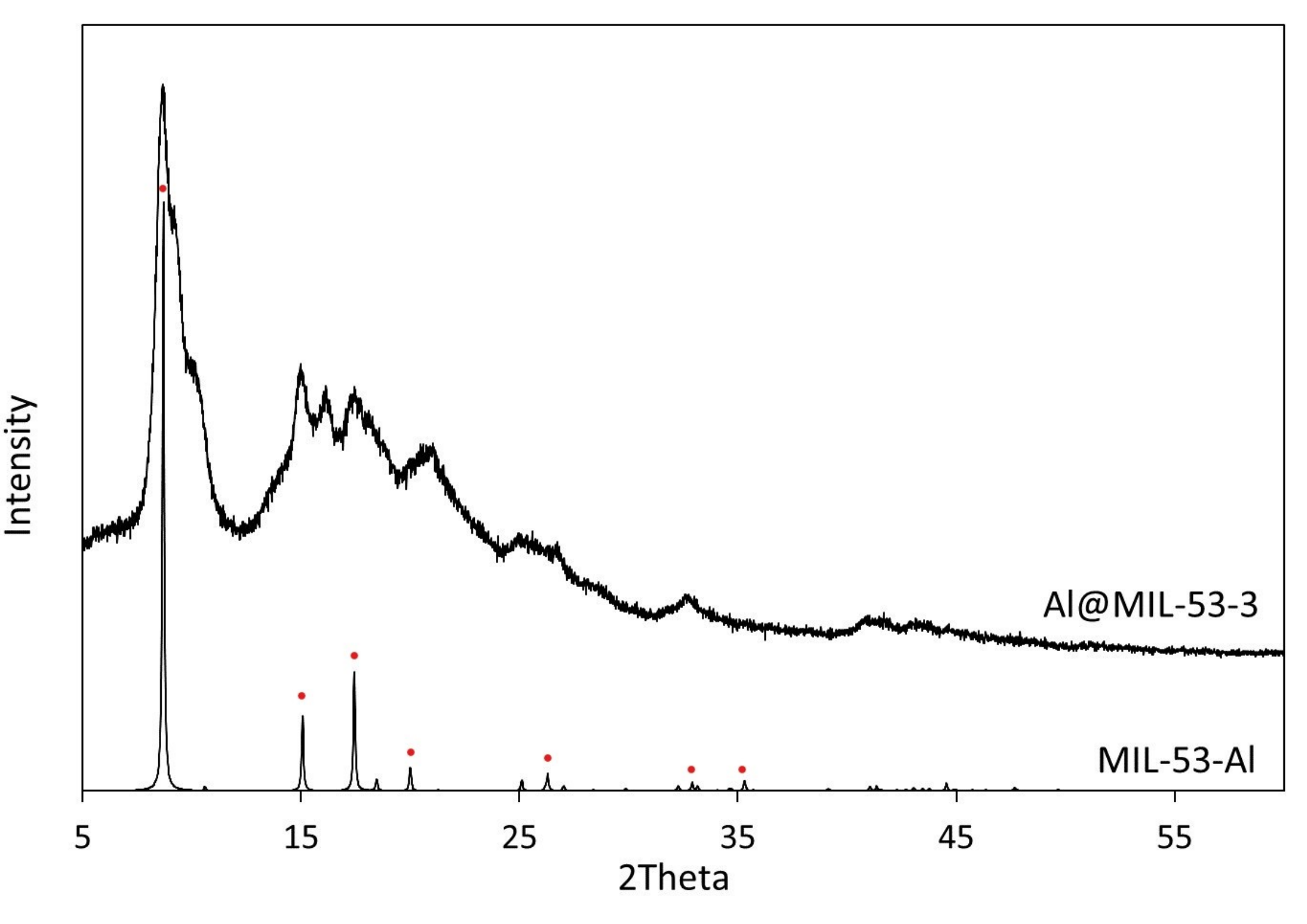
Intensity
Al@MIL-53-3
MIL-53-Al
5
15
25
35
45
55
2Theta

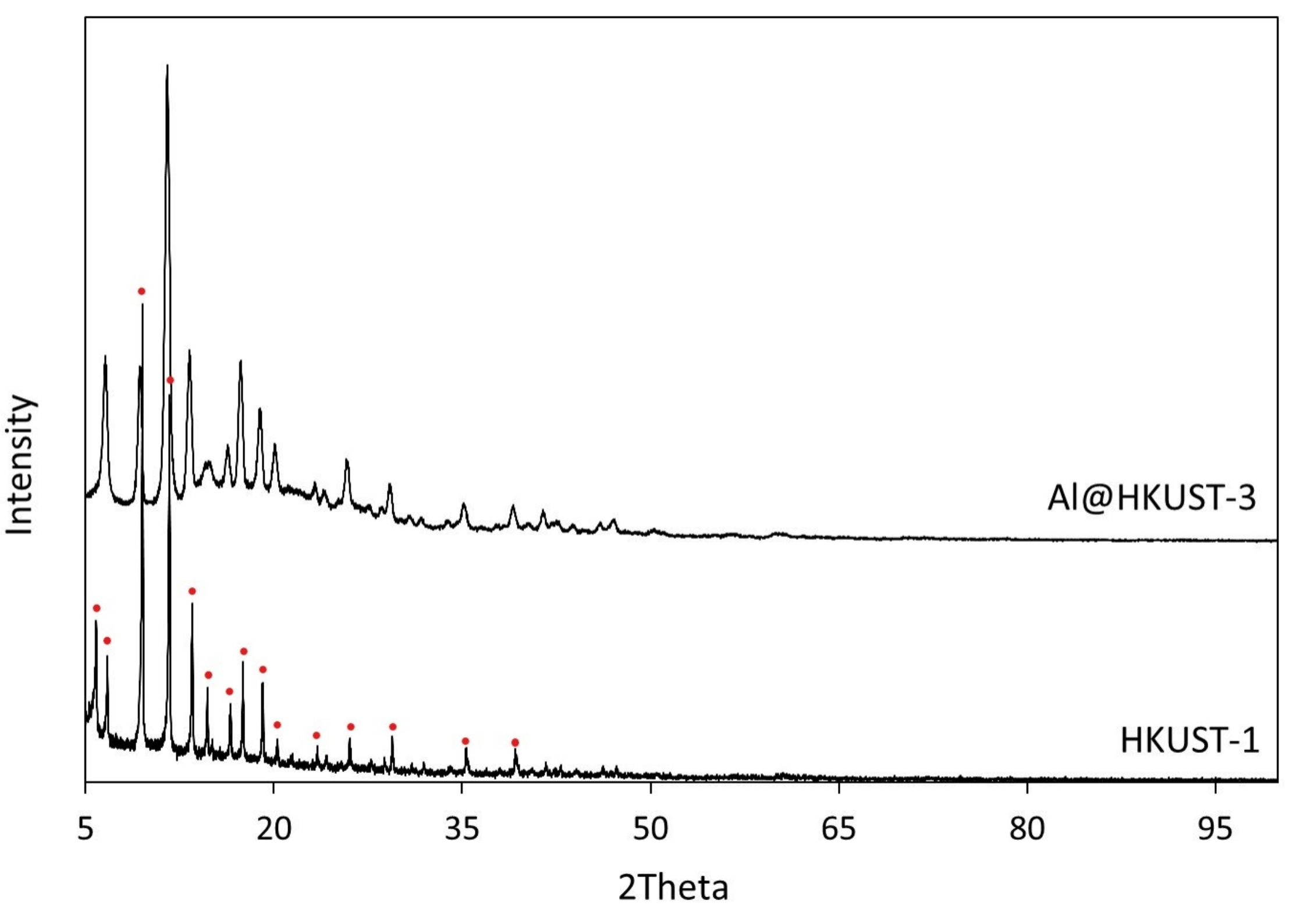
Intensity
Al@HKUST-3
HKUST-1
5
20
35
50
65
80
95
2Theta

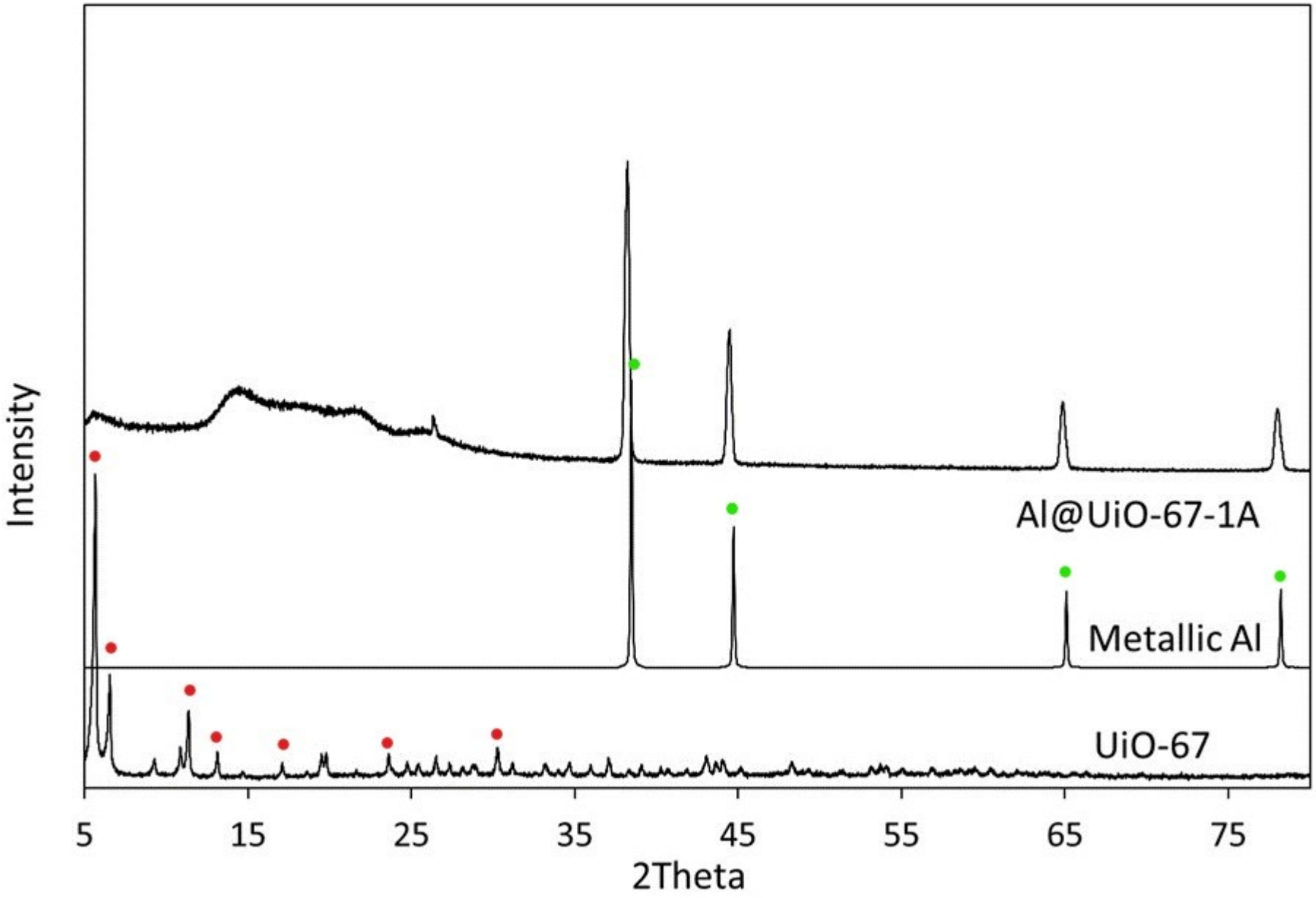
Intensity
Al@UiO-67-1A
Metallic Al
UiO-67
5
15
25
35
45
55
65
75
2Theta

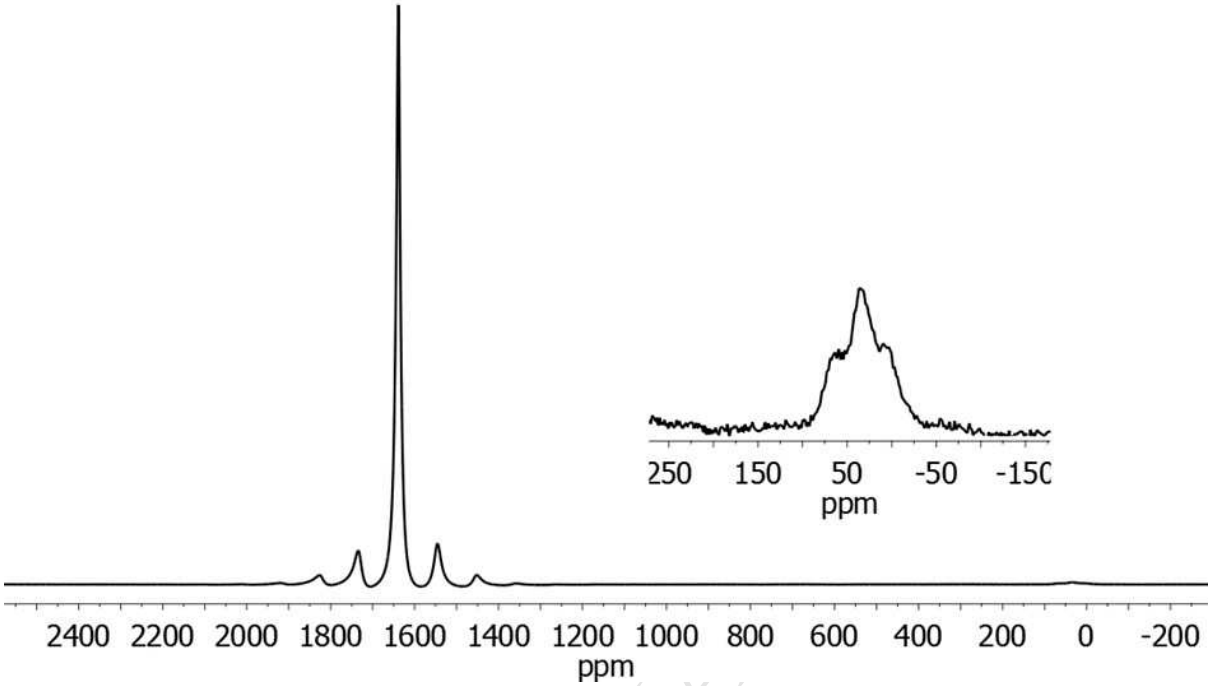

Highlights

- Impregnation of Al in three different metal-organic frameworks (MOFs).
- Simple impregnation procedure using AlH_3•NMe_2Et, heat, and vacuum.
- Theoretical loadings were calculated from atomic, molecular and pore volumes.
- Impregnation into UiO-67 gave Al(0) crystals of ca. 30 nm.
- UiO-67 framework decomposed, but still provided protection from oxidation.